

Evaluating Deep Clustering Algorithms on Non-Categorical 3D CAD Models

Siyuan Xiang^{* ‡} Chin Tseng^{* ‡} Congcong Wen[‡] Deshana Desai[‡] Yifeng Kou[‡]
 Binil Starly[§] Daniele Panozzo[‡] Chen Feng^{† ‡}

[‡]New York University [§]Arizona State University

<https://cluster3d.github.io/>

Abstract

We introduce the first work on benchmarking and evaluating deep clustering algorithms on large-scale non-categorical 3D CAD models. We first propose a workflow to allow expert mechanical engineers to efficiently annotate 252,648 carefully sampled pairwise CAD model similarities, from a subset of the ABC dataset with 22,968 shapes. Using seven baseline deep clustering methods, we then investigate the fundamental challenges of evaluating clustering methods for non-categorical data. Based on these challenges, we propose a novel and viable ensemble-based clustering comparison approach. This work is the first to directly target the underexplored area of deep clustering algorithms for 3D shapes, and we believe it will be an important building block to analyze and utilize the massive 3D shape collections that are starting to appear in deep geometric computing.

1. Introduction

Clustering and classification are two ways to recognize repeated patterns in large-scale 3D model datasets, which could serve downstream applications like 3D data management, compression, search, and exploration [3, 12, 16, 30]. Currently, the community is focusing more on categorical dataset [6, 32] for 3D object classification tasks [24, 25, 28]. However, sometimes the data distribution, especially in large-scale CAD datasets, might be very complex, and class labels are very difficult to assign, making it hard to train and evaluate shape classification. ABC dataset [19] is an example of such type of dataset, which is composed of 1 million 3D CAD models manually modeled by hobbyists and experts alike. *One may easily understand the difficulty of the classification task by trying to assign names to each group of objects in Figure 1*, and more challenge details are in the Section 2 and supplementary. Therefore, we have to explore clustering-based analysis of such datasets.

To the best of our knowledge, we are the first to explore the deep clustering algorithms on such a non-categorical 3D model dataset. We first establish a benchmark, adopting classic or state-of-the-art deep clustering algorithms on the dataset. More importantly, we propose a strategy for evaluating these methods. Previously, the external evaluation principles for most of the clustering algorithms in vision and learning community are based on class labels [4, 35], which oversimplifies the inter-cluster and intra-cluster object similarity and does not apply to our case. Differently, our evaluation strategy directly examines the pairwise similarity relationships between every two CAD models. For this evaluation system, we propose a scalable and effective pairwise similarity annotation workflow and implement a graphical user interface for efficient human annotations. Based on the pairwise similarity, we propose a novel ensemble-based clustering evaluation protocol to rank the clustering algorithms.

For creating the deep clustering benchmark on non-categorical 3D models, we select a subset in ABC dataset [19], adapting seven unsupervised deep clustering methods to the subset. These clustering methods can be classified into two types: (1) two-stage clustering and (2) end-to-end deep clustering. For the two-stage clustering approach, we first perform deep representation learning on 3D mechanical components to extract high dimensional features, using pre-trained neural networks. Then we apply classic clustering algorithms, like KMeans [21], to group these learned features into different clusters. For end-to-end deep clustering methods, we combine representation learning, dimensionality reduction, and clustering in an end-to-end framework.

For the evaluation protocol, instead of using class labels, we ask expert annotators (graduate students in mechanical engineering) to label pairwise 3D shape similarity relationships between each pairs of 3D models as the external knowledge for evaluation. But annotating all the pairs is obviously intractable: a rough estimate is that a single annotator working 24 hours a day would need 16 years to annotate the 500 millions of edges in our dataset! As a compromise,

^{*}Equal contribution.

[†]The corresponding author is Chen Feng cfeng@nyu.edu.

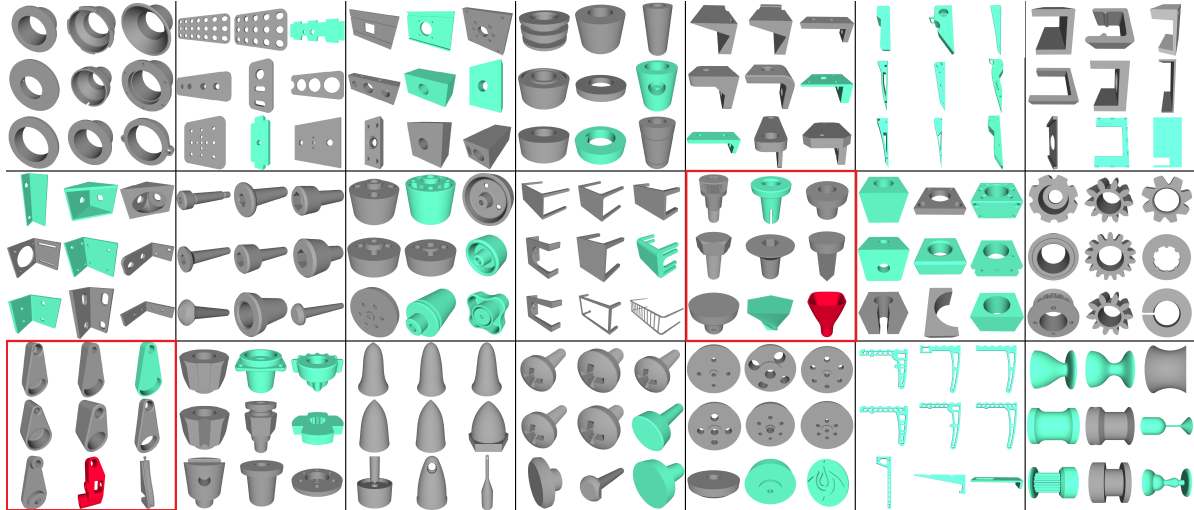


Figure 1. **The overview of our work** via a subset of clustering results from a baseline (DeepCluster [4]). It demonstrates the challenges of classification-based labeling in our task, due to many non-standard mechanical components (green). Each section shows some random CAD models in the same cluster. A red section shows a cluster with annotation violations highlighted at the red objects.

we propose a workflow to carefully select a small subset of non-trivial pairs to obtain useful annotations. We developed a web-based user interface using this workflow and annotated 252,648 selected pairwise similarities on 22,968 ABC shapes.

However, because of the relatively sparse annotation compared to annotating all the pairs, we find that bias is inevitable so we cannot rely only on these human annotations for a fair evaluation of baselines. Trying to tackle *this dilemma, where full annotation is intractable and sparse annotation is unfair*, we propose a novel clustering evaluation protocol based on the ensemble principle [36].

Instead of trying to find an “absolute” ranking of baselines by comparing them to an unobservable ground truth, *our evaluation protocol is “relative, dynamic, and democratic”* by using the ensemble of different similarity predictions and human annotations as an approximation of that ground truth. Our justification for this evaluation protocol is based on the general consensus of the reduced variance and improved robustness/accuracy of ensemble-based system [36], and also our various experimental evidences.

We believe that our evaluation strategy is useful to provide an objective metric on clustering tasks on non-categorical dataset. *Because of the uniqueness of our protocol, we plan to continue collecting data and clustering methods, periodically updating the benchmark.* The human annotations and benchmark results, the annotation software, all baseline implementations, and the evaluation scripts will be publicly released as open source using the MIT license.

In summary, our contributions are the following:

- To the best of our knowledge, it is the first work focusing on deep clustering for non-categorical 3D shapes, which could stimulate a new direction for 3D deep clustering.

- We propose a scalable and effective pairwise similarity annotation workflow, implemented in a graphical user interface, to allow experts to efficiently label a large number of non-trivial 3D object pairwise similarity (for a total of 252,648 annotation pairs per annotator).
- We adapt 7 deep clustering algorithms for 3D CAD models, creating the first 3D deep clustering benchmark.
- We propose a novel ensemble-based clustering evaluation protocol for non-categorical data, with experimental justifications using 7 baseline clustering methods and several internal evaluation indices.

2. Related Work

We cover the related works more closely related to our main contributions: (1) clustering algorithms and corresponding evaluation metrics, (2) large datasets of 3D models, and (3) approaches for annotating 3D datasets.

3. Annotation Creation

3.1. Human annotation

We view the selected subset from ABC dataset as an undirected complete graph $\mathcal{G}(\mathcal{V}, \mathcal{E})$. The node set \mathcal{V} contains all the 3D CAD models in the subset, each one is a node $v \in \mathcal{V}$. We denote the cardinality of the set as $|\mathcal{V}|$. An edge $e_{i,j} \in \{+1, -1, 0\}$ in the edge set \mathcal{E} stores the similarity annotation of two 3D CAD models v_i and v_j . The edge labels $+1, -1$, and 0 respectively indicate similar, dissimilar, and unknown relationship between two nodes. The edge set can come from human annotation or from a clus-

tering algorithm. Next, we introduce how we create and annotate the subset, and then discuss several important design considerations.

3.1.1 Annotation creation workflow

We use the workflow illustrated in Figure 2 with the following major steps:

Step 1: Data Cleaning. We use the first four chunks of the ABC dataset [19], and filter out all blank files and all files containing assemblies instead of single components, obtaining a subset of 22,968 CAD models.

Step 2: Similarity Annotation. While ideally we would like to manually annotate each edge, this is not practical. We thus introduce a method to carefully sample a subset of edges that will be manually annotated.

Step 2.1: Cluster Initialization. We group all the CAD models into a set of initial clusters $\mathcal{C}_{\mathcal{I}} \equiv \{\mathcal{C}_k \mid \cup_{\forall k} \mathcal{C}_k = \mathcal{V}; \mathcal{C}_k \cap \mathcal{C}_l = \emptyset, \forall k \neq l; \text{ and } |\mathcal{C}_k| \leq T, \forall k\}$, each containing no more than $T = 12$ CAD models, using a clustering method detailed in Section 3.2. The number 12 is chosen to facilitate a comfortable and useful labeling by humans in the graphical interface, because they can easily see the details of each model and still be able to compare each other efficiently at a glimpse. We then automatically assigned label 0 (meaning unknown) to all the edges across different clusters, i.e., $e_{i,j} = 0 \iff v_i \in \mathcal{C}_k, v_j \in \mathcal{C}_l, \text{ and } k \neq l$.

Step 2.2: Human Annotation. We only manually annotate edges residing inside the same initial cluster, i.e., $e_{i,j} \neq 0 \iff \exists \mathcal{C}_k \in \mathcal{C}_{\mathcal{I}}, v_i \in \mathcal{C}_k, v_j \in \mathcal{C}_k$. A number of $A = 4$ mechanical engineers served as our experts to provide their CAD model similarity annotations independently. For each initial cluster, e.g., \mathcal{C}_k , an annotator has to either *confirm* that CAD models inside \mathcal{C}_k are all similar to each other, or further *divide* the cluster into smaller clusters until such confirmations can be made for each smaller cluster. The *confirmation* of a cluster \mathcal{C}_l assigns all internal edges inside this cluster with the *positive* label +1, i.e., $e_{i,j} = +1 \iff v_i \in \mathcal{C}_l, v_j \in \mathcal{C}_l$. The *division* of a cluster \mathcal{C}_l into smaller clusters $\{\mathcal{C}_{l_s} \mid \cup_{\forall t} \mathcal{C}_{l_t} = \mathcal{C}_l; \mathcal{C}_{l_s} \cap \mathcal{C}_{l_t} = \emptyset, \forall s \neq t\}$ assigns all edges across those small clusters with the *negative* label -1, i.e., $e_{i,j} = -1 \iff v_i \in \mathcal{C}_{l_t}, v_j \in \mathcal{C}_{l_s}, s \neq t$. We record each annotator independently, i.e., the a -th annotator’s annotation forms an edge set \mathcal{E}^a over the same nodes. The instruction information is in the supplementary.

3.2. Design Decisions on the Annotation Workflow

Although it has been widely used in geometry processing and machine learning, the concept of similarity can be vague and ambiguous when applied to 3D CAD models in Cluster3D.

Why manually annotate similarity? To determine whether two 3D models are similar or not algorithmically,

there are two main criteria: geometric distribution similarity [11, 15, 22, 27] and visual similarity [7]. Yet for human beings, the mechanism to determine the similarity between two CAD models is also based on unconscious background knowledge [9, 34], which might be different from the similarity judgment encoded in existing algorithms [8, 34]. Therefore, acquiring large-scale human annotations for pairwise CAD model similarity is still important to capture experts’ underlying background knowledge. In our practice, annotators are only given 3D CAD models, without extra information like material or size. Therefore, in most cases human annotation is determined by the geometric information.

Reasons for cluster initialization. It is impractical for human experts to annotate the similarity relationships between all pairs of CAD models, as their number is quadratic with respect to the number of models considered. It would take 16 years of annotation time, assuming a 1 second time to annotate each edge.

Therefore, we have to commit to annotate only a small subset of edges. The most obvious and unbiased approach is to random sample from all the edges. This is however not an option for our case, as the sampling would be too unbalanced, as most of the edges indicate dissimilarity between objects. We needed a strategy that would give us a more or less even split between similar and dissimilar edges so that we could use our expert time meaningfully and evaluate clustering methods in a balanced way.

After experimenting with different approaches, we found a method that leads to a reasonable 1 to 1 ratio of similar and dissimilar edges in our dataset: we use a clustering algorithm to over segment the dataset in small clusters (12 objects/cluster), and then ask users to annotate all edges within each cluster. Overall, this approach allowed us to get a good distribution of edge labels while annotating about only 0.5% of the entries in our similarity matrix, making the annotation problem tractable with our budget and resources.

Cluster initialization and evaluation bias. A natural question is how to use this extremely sparse annotation to evaluate baseline clustering methods, because the different choices of cluster initialization would lead to a different subset of annotated edges. Will this inevitably introducing bias if we directly use the annotations for evaluation? Or will we obtain consistent evaluation even if the cluster initialization is different? *To answer this question in our experiment section, we use two different methods for cluster initialization: the MVCNN [29]-based method and the AtlasNet [14]-based method, which leads to different subsets of edges for annotation.*

For the MVCNN-based method, we first generate 12 images for all 22,968 CAD models in our dataset, following the original settings in [29]. We use all these $12 \times 22,968$ images to train a convolutional auto-encoder network. Then

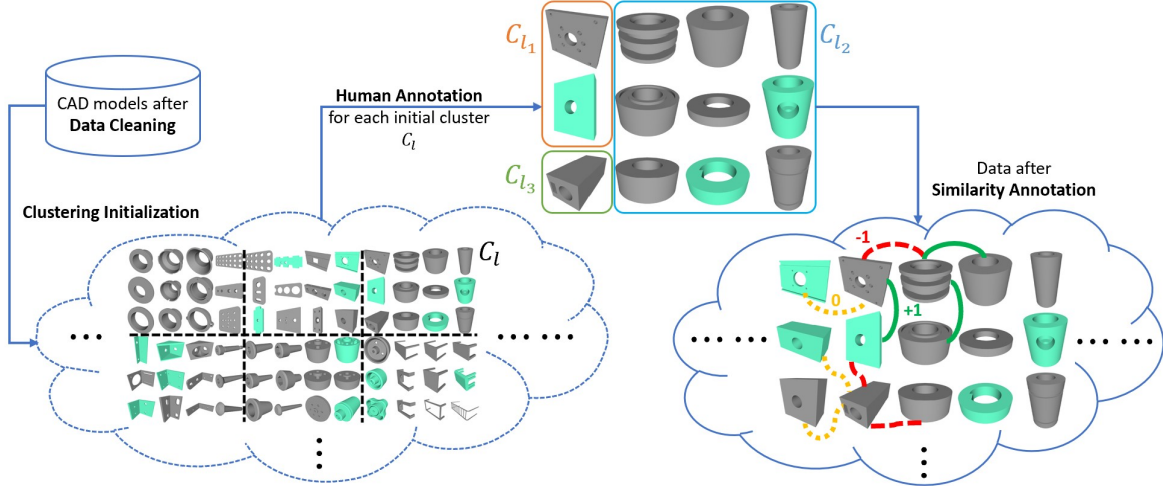


Figure 2. Human annotation workflow.

the trained encoder is used to extract features for all these images. For each CAD model, we concatenate the twelve latent vectors from its corresponding 12 images to represent its features. For the *AtlasNet-based method*, we follow the original auto-encoder architecture to reconstruct 3D point cloud for each input 3D CAD object, and then predict the features for each CAD model using the encoder of the trained model.

Finally, for both methods, 22,968 features representing all shapes in Cluster3D are clustered by KMeans algorithm. With the number of clusters K in KMeans set to 2,000, we obtain two thousand initial clusters for the human annotators. We continue to split the clusters with more than 12 models in the class using KMeans, until the contained number of models is no greater than 12. These clustered CAD models are then loaded into our annotation interface.

Annotation interface. We developed a web-based annotation application. The interface shows CAD models of one cluster at a time. It shows the 12 CAD models with checkbox, and initially all 12 checkbox are set to be checked. The annotators manually unmark the models which are considered dissimilar from the others, effectively annotating all edges linking the 12 models in the cluster. After confirmation, a new set of 12 models is shown. We will show our web interface in the supplementary.

Data statistics. The selected CAD model subset has 22,968 CAD models; therefore, there are $22,968 \times 22,967/2$ similar or dissimilar edges in total between every two CAD models. We have four human experts to annotate two different edge subsets due to different cluster initialization, and each initial cluster contain 252,648 edges to be labeled. This leads to eight different human annotation edge sets \mathcal{E}^a . The statistics of average annotation consistency between different human experts is above 70%; there-

fore, we believe it is reasonable to use these human annotations, especially after using majority voting strategy (details in Section 4.3). More statistics for annotation consistency between different human experts, *positive* and *negative* labels for each expert can be found in the supplementary.

4. Benchmark

4.1. Baseline methods

Based on the availability and usability of source codes, we select and adapt seven baseline methods to establish a benchmark for clustering algorithms. We divide these baseline methods into two types: (1) two-stage clustering, and (2) end-to-end deep clustering. Two-stage clustering methods use a deep neural network to extract features for all CAD models, then apply a traditional clustering algorithm, such as KMeans. End-to-end deep clustering baseline methods integrate feature extraction and clustering in one framework: during the training process both network loss and clustering loss are minimized. Note that all these methods are considered as partitional clustering [5], i.e. one CAD model will only fall into one cluster.

Since some of the baseline methods are designed for 2D images, we adapt them for 3D CAD models. We use either point cloud or multi-view images as the input representation, and select suitable deep neural networks. A detailed description of all network architectures can be found in the supplementary.

Two-stage clustering. Also used for cluster initialization, *MVCNN* [29] and *AtlasNet* [14] have been described in Section 3. We add one more baseline in this group, *BYOL* [13]: BYOL is proposed to compute self-supervised image representation learning. We replace the image encoder (ResNet) with a point cloud encoder (PointNet) to

learn a representation of a 3D CAD shape. We use three types of data augmentation on point cloud: random dropout, random scaling, and random shift. We then apply the KMeans algorithm on the learned latent representation to cluster CAD objects.

End-to-end deep clustering. Four methods are selected in this group.

DEC [33]: To adapt the DEC algorithm, we initialize DEC with the AtlasNet architecture to auto-encode 3D point clouds as the input data. The deep auto-encoder is trained to minimize Chamfer loss and learns representations of the 3D shapes. We then follow the DEC algorithm by discarding the decoder layers and use the encoder layers as the initial mapping between the data and feature space. This is followed by joint optimization of the cluster centers and encoder parameters using SGD with momentum.

DeepCluster [4]: We replace the convolution networks trained by the DeepClustering algorithm to use PointNet instead for encoding the point cloud data to predict cluster assignments. The algorithm is followed by alternating between clustering of the point cloud feature descriptors using K-Means and training the PointNet network using the multinomial logistic loss function.

IIC [18]: Instead of the original IIC method for unsupervised image semantic task, we first randomly transform a CAD model to a pair of point clouds, and use PointNet as encoder to maximize mutual information between the class assignments of each pair. The trained model directly outputs class labels for each 3D CAD model.

SCAN [31]: We adjust the pretext stage: Instead of using noise contrastive estimation (NCE) to determine the nearest neighbors, we use the auto-encoder of AtlasNet we have trained to output the feature vectors to generate the nearest neighbors set.

4.2. Evaluation Metrics

As discussed in Section 2, external and internal evaluation indices are used for evaluating clustering results.

External evaluation indices. We evaluate the clustering results of the baseline methods using two external evaluation indices: *edge accuracy* and *balanced accuracy*. *Edge accuracy* is the binary similarity classification accuracy for each edge compared to a ground truth similarity matrix. For the clustering results obtained from the baseline methods, the CAD models grouped into the same cluster are considered as pairwise similar, thus predicting the edges between these models as +1. The predicted edges between models in different clusters are considered as -1. We calculate the average classification accuracy for all the edges as *edge accuracy*. However, in practice, most of the CAD models are dissimilar to each other, which means most of the edges have ground truth labels as -1. Therefore, the dataset is heavily imbalanced. To better evaluate the baseline meth-

ods’ performance, we use balanced accuracy [2], which suffer less from the imbalance. More calculation details are available in the supplementary.

Internal evaluation indices. We opt for the silhouette coefficient [26] method, which is widely used in clustering problems. Based on its definition, we need to determine the distance between every two objects. In our dataset, the objects are 3D CAD models which can be represented as point cloud or voxel grids. Therefore, we choose to use the Chamfer distance [10] and the Jaccard distance [20] as two distances between CAD models.

4.3. Ensemble-based Evaluation

As discussed, when we use external evaluation indices, a ground truth similarity matrix is needed. Because the full ground truth is intractable to be annotated, one naive way is to directly use the sparsely annotated similarity matrix from Section 3.1.1, which could lead to biased evaluation. Another way is to ensemble multiple similarity matrices as a proxy of the full ground truth matrix.

The ensemble similarity matrix (denoted *Ensemble*) is generated by combining n different similarity matrices using a majority voting strategy. Similarly as the human annotation result matrix, the *Ensemble* matrix can be viewed as an edge set over the graph. However, unlike the sparse human annotation matrix where many entries are zero, any clustering method predicts a dense matrix where each edge is known, and the edge labels either indicate similar, or dissimilar, as $e_{i,j} \in \{+1, -1\}$. Next, we will describe how we create the *Ensemble* matrix, and why we think it is reasonable to use it.

Individual similarity matrix. In this paper, each individual similarity matrix is independently created by the clustering result of a selected clustering method. For example, a clustering method can group all the CAD models into non-overlapping K groups, as $\{\mathcal{C}_k | \cup_{\forall k} \mathcal{C}_k = \mathcal{V}, \mathcal{C}_k \cap \mathcal{C}_l = \emptyset \text{ and } \forall k \neq l, \forall k\}$. Within each group \mathcal{C}_k , all the CAD models are considered as similar to each other, thus, $e_{i,j} = +1 \iff v_i \in \mathcal{C}_k, v_j \in \mathcal{C}_k$. Meanwhile, the CAD models in different groups are considered as dissimilar to each other, thus the edge labels are *negative*, $e_{i,j} = -1 \iff v_i \in \mathcal{C}_k, v_j \in \mathcal{C}_l, k \neq l$.

Ensemble by majority voting. After obtaining N different $|\mathcal{V}| \times |\mathcal{V}|$ similarity matrices using various baseline clustering methods, we use the majority voting strategy to ensemble all the label decisions for each edge, leading to the *Ensemble* matrix. For each edge $e_{i,j}$, there are N labels from N similarity matrices. We define the final label of $e_{i,j}$ as the +1 if the number of *positive* labels of $e_{i,j} \geq \lceil \frac{N+1}{2} \rceil$, otherwise -1.

We further consider to use human annotations for the evaluation protocol. As mentioned, in our study, we have eight different annotations from four annotators and two

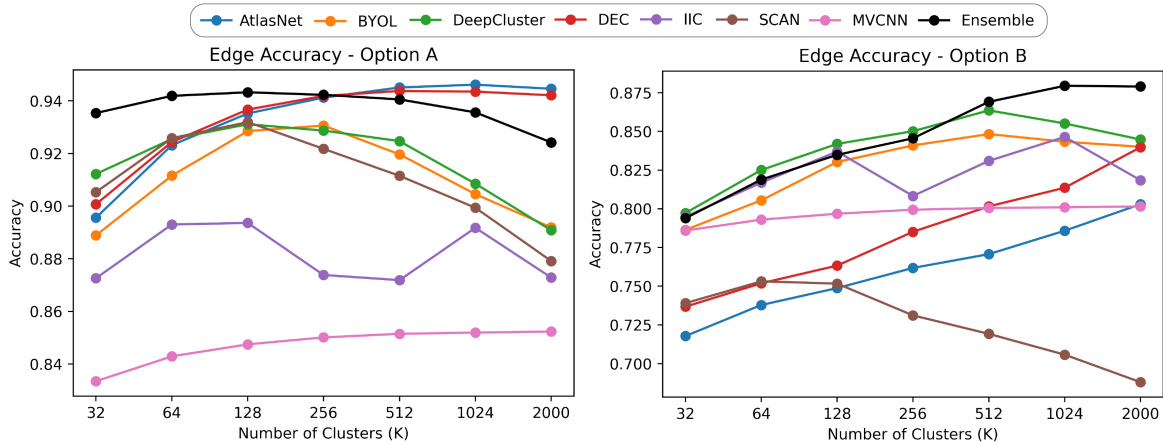


Figure 3. **Evaluation bias when using Human alone**, based on different cluster initialization from MVCNN (option-A) and AtlasNet (option-B).

different edge subsets. We create the human ensemble matrix (denoted *Human*) by the same majority voting strategy. Note that if for an edge $e_{i,j}$, four annotators annotate it as +1, and the remaining four annotators annotate it as -1, we will consider this edge as unknown with a label 0. Finally, we calculate the balanced accuracy using *Ensemble* and *Human* separately. We also average the two accuracy values, and denote it as *EnsembleHuman*.

Justification for the ensemble-based evaluation. The ensemble by majority voting trusts the most frequently predicted edge labels among all methods/annotations. Given that the full ground truth cannot be obtained with reasonable human investment, such a proxy is a reasonable approximation for two reasons: (1) the ensemble is a commonly accepted strategy to reduce variance, enhance robustness, and therefore, improve accuracy [36] (the ensemble results are often empirically closer to ground truth) and (2) our experimental results in Figure 3 also support this choice, as we will detail in Section 5.

5. Experiments and Discussions

Experiment settings. All the baseline methods are implemented using PyTorch [23] and run on an NVIDIA GeForce GTX 1080 Ti GPU. For hyperparameter settings, we tune learning rate and batch size for each baseline method. The learning rates for MVCNN-based method, AtlasNet-based method, BYOL-based method, DEC, DeepCluster, IIC, and SCAN are 0.0001, 0.001, 0.0003, 0.00001, 0.05, 0.0003, and 0.0001 respectively. The batch sizes for these methods are 60, 11, 10, 128, 50, 10, and 96 respectively.

Since we do not know a proper number of clusters in ABC, we select seven different number of clusters (K), from 32 to 2,000, following exponential growth, and we evaluate all methods on all these cases independently.

Bias of cluster initialization. One question was raised in Section 3.2 regarding the potential evaluation bias of using different cluster initialization methods to select the edge subsets for manual annotation. To evaluate that, we compare the similarity matrices of the human annotators initialized by the MVCNN-based method and the AtlasNet-based method to the similarity matrices obtained with various baseline methods in Figure 3. *The resulting baseline rankings are inconsistent between the two initialization methods, indicating that the choice of initial clustering method indeed introduces an evaluation bias.* This bias is due to the small number of annotated edges, and thus it is not fair to directly use the human annotated sparse similarity matrices to compare different clustering algorithms.

Empirical justification of the ensemble method. Figure 3 also shows that ensemble method has the highest accuracy (on average over the different K) than all baselines. Furthermore, there are only about 6% of human annotations in conflict with the result of the ensemble method, showing that it has a high degree of agreement with the human annotations.

Ensemble-based external evaluation indices. We use balanced accuracy, instead of edge accuracy because both *Ensemble* and *EnsembleHuman* are imbalanced, containing more *negative* edges than *positive* edges. We plot the balanced accuracy results using both ensemble matrices (*Ensemble* and *EnsembleHuman*) as reference in Figure 4. We find that the two different evaluation results show a consistent ranking of baseline methods, although adding human annotations into evaluation slightly changes the absolute balanced accuracy for the baseline methods. Such a ranking consistency is a good evidence supporting our ensemble-based protocol for our clustering evaluation challenge.

End-to-end deep clustering methods do not necessarily outperform two-stage clustering methods. As shown in Figure 4, for our task there is no major advantage for using end-

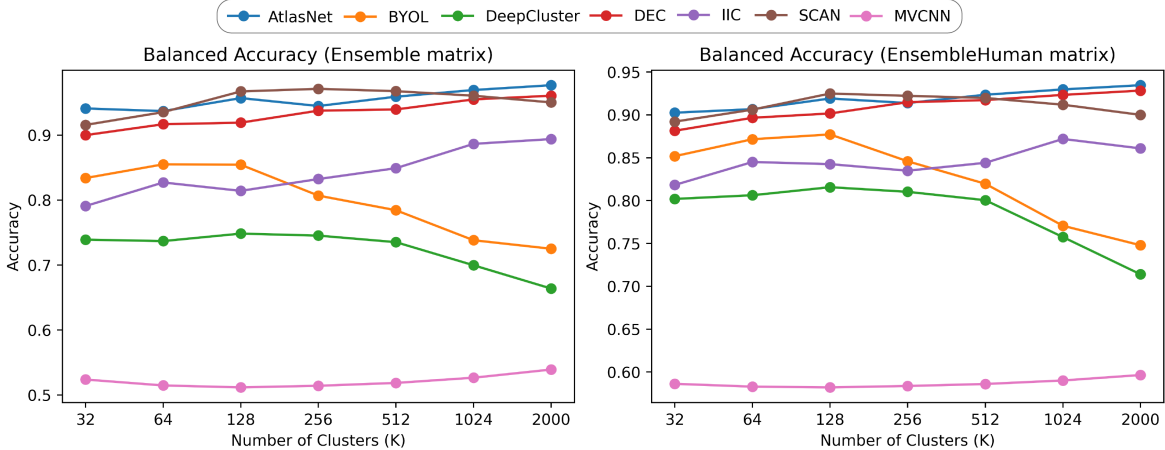


Figure 4. **Consistent ensemble-based external evaluation indices.** Rank of balanced accuracy for both *Ensemble* and *EnsembleHuman*: AtlasNet > SCAN > DEC > IIC > BYOL > DeepCluster > MVCNN.

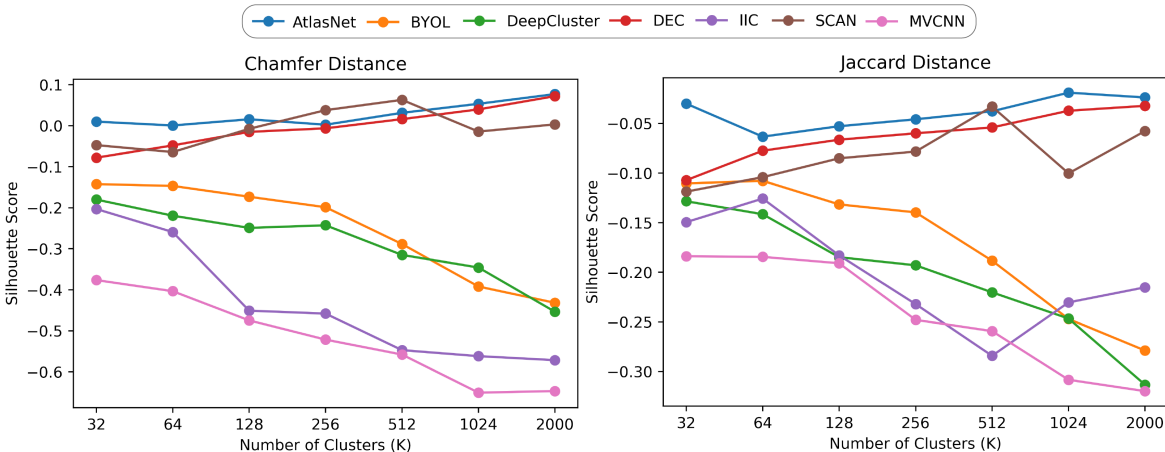


Figure 5. **Benchmark results of internal evaluation indices.** Chamfer ranking: AtlasNet > SCAN > DEC > BYOL > DeepCluster > IIC > MVCNN; Jaccard ranking: AtlasNet > DEC > SCAN > BYOL > IIC > DeepCluster > MVCNN.

to-end methods (DeepCluster, DEC, IIC, SCAN), compared to two-stage clustering methods (AtlasNet-based method, BYOL-based method, MVCNN-based method). Therefore, we believe it is necessary to study how to take the advantage of the clustering loss we use to train deep neural models.

The MVCNN-based method has the lowest accuracy. We believe the different performance is due to the fact that it uses a different representation: images instead than point clouds. This suggests that in our dataset where class supervision does not exist and shape distribution is diverse, point-cloud-based unsupervised representation learning might be more effective than image-based ones.

Clustering results using internal evaluation indices. Figure 5-(Chamfer distance) shows the benchmark results using the *silhouette score* as internal evaluation index. Using the Chamfer and Jaccard distances lead to similar performances. For all methods, we find that the clusters are not

obviously different or even wrongly assigned, since most of the silhouette score is below 0. Another interesting observation is that the AtlasNet-based method, DEC, and SCAN methods perform better when the number of cluster K increases, while other baseline methods show the opposite trend, which clearly shows which baselines perform better.

The baseline performances are mostly consistent in external and internal evaluation indices. Comparing Figure 4 and Figure 5, we find that the ranking of the baseline methods are very consistent. The top three ranked methods are always AtlasNet-based method, SCAN, and DEC no matter using which indices. The DeepCluster and MVCNN-based methods are always performing badly in Cluster3D. This consistency is an additional evidence supporting our proposed ensemble-based evaluation protocol.

5.1. Limitations and discussion

The major challenge in our study is that it is not possible, for practical reasons, to have a fully annotated ground truth to rank the different baseline methods. Our approach based on an ensemble method is a proxy, justified by our experiments, that is likely to be a good approximation, but it is still an approximation. To increase the quality of this approximation, we can either add more data or more methods to improve the quality of the ensemble approximation, both directions that we are planning to explore as future work.

6. Conclusion

This is the first work for the development and evaluation of clustering algorithms on collections of 3D CAD models. We introduce the annotated data, the ensemble matrix for evaluation, and evaluated seven clustering methods using both external and internal evaluation indices. We believe our work will be an important resource to develop and evaluate new clustering methods tailored for 3D geometry.

References

- [1] Nikhil Bansal, Avrim Blum, and Shuchi Chawla. Correlation clustering. *Machine learning*, 56(1):89–113, 2004. 11
- [2] Kay Henning Brodersen, Cheng Soon Ong, Klaas Enno Stephan, and Joachim M Buhmann. The balanced accuracy and its posterior distribution. In *2010 20th international conference on pattern recognition*, pages 3121–3124. IEEE, 2010. 5, 13
- [3] Benjamin Bustos, Daniel Keim, Dietmar Saupe, and Tobias Schreck. Content-based 3d object retrieval. *IEEE Computer Graphics and Applications*, 27(4):22–27, 2007. 1
- [4] Mathilde Caron, Piotr Bojanowski, Armand Joulin, and Matthijs Douze. Deep clustering for unsupervised learning of visual features. In *Proceedings of the European Conference on Computer Vision (ECCV)*, pages 132–149, 2018. 1, 2, 5
- [5] M Emre Celebi. *Partitional clustering algorithms*. Springer, 2014. 4
- [6] Angel X Chang, Thomas Funkhouser, Leonidas Guibas, Pat Hanrahan, Qixing Huang, Zimo Li, Silvio Savarese, Manolis Savva, Shuran Song, Hao Su, et al. Shapenet: An information-rich 3d model repository. *arXiv preprint arXiv:1512.03012*, 2015. 1
- [7] Ding-Yun Chen, Xiao-Pei Tian, Yu-Te Shen, and Ming Ouhyoung. On visual similarity based 3d model retrieval. In *Computer graphics forum*, volume 22, pages 223–232. Wiley Online Library, 2003. 3
- [8] Florin Cutzu and Shimon Edelman. Representation of object similarity in human vision: psychophysics and a computational model. *Vision research*, 38(15-16):2229–2257, 1998. 3
- [9] Hans P Op de Beeck, Katrien Torfs, and Johan Wagemans. Perceived shape similarity among unfamiliar objects and the organization of the human object vision pathway. *Journal of Neuroscience*, 28(40):10111–10123, 2008. 3
- [10] Haoqiang Fan, Hao Su, and Leonidas J Guibas. A point set generation network for 3d object reconstruction from a single image. In *Proceedings of the IEEE conference on computer vision and pattern recognition*, pages 605–613, 2017. 5
- [11] Thomas Funkhouser, Patrick Min, Michael Kazhdan, Joyce Chen, Alex Halderman, David Dobkin, and David Jacobs. A search engine for 3d models. *ACM Transactions on Graphics (TOG)*, 22(1):83–105, 2003. 3
- [12] Yue Gao, Meng Wang, Dacheng Tao, Rongrong Ji, and Qionghai Dai. 3-d object retrieval and recognition with hypergraph analysis. *IEEE Transactions on Image Processing*, 21(9):4290–4303, 2012. 1
- [13] Jean-Bastien Grill, Florian Strub, Florent Altché, Corentin Tallec, Pierre H Richemond, Elena Buchatskaya, Carl Doersch, Bernardo Avila Pires, Zhaohan Daniel Guo, Mohammad Gheshlaghi Azar, et al. Bootstrap your own latent: A new approach to self-supervised learning. *arXiv preprint arXiv:2006.07733*, 2020. 4
- [14] Thibault Groueix, Matthew Fisher, Vladimir G Kim, Bryan C Russell, and Mathieu Aubry. A papier-mâché approach to learning 3d surface generation. In *Proceedings of the IEEE conference on computer vision and pattern recognition*, pages 216–224, 2018. 3, 4
- [15] Masaki Hilaga, Yoshihisa Shinagawa, Taku Kohmura, and Toshiyasu L Kunii. Topology matching for fully automatic similarity estimation of 3d shapes. In *Proceedings of the 28th annual conference on Computer graphics and interactive techniques*, pages 203–212, 2001. 3
- [16] Tianxin Huang and Yong Liu. 3d point cloud geometry compression on deep learning. Association for Computing Machinery, 2019. 1
- [17] Krishna Murthy Jatavallabhula, Edward Smith, Jean-Francois Lafleche, Clement Fuji Tsang, Artem Rozantsev, Wenzheng Chen, Tommy Xiang, Rev Lebaredian, and Sanja Fidler. Kaolin: A pytorch library for accelerating 3d deep learning research. *arXiv:1911.05063*, 2019. 10
- [18] Xu Ji, João F Henriques, and Andrea Vedaldi. Invariant information clustering for unsupervised image classification and segmentation. In *Proceedings of the IEEE/CVF International Conference on Computer Vision*, pages 9865–9874, 2019. 5
- [19] Sebastian Koch, Albert Matveev, Zhongshi Jiang, Francis Williams, Alexey Artemov, Evgeny Burnaev, Marc Alexa, Denis Zorin, and Daniele Panozzo. Abc: A big cad model dataset for geometric deep learning. In *Proceedings of the IEEE/CVF Conference on Computer Vision and Pattern Recognition*, pages 9601–9611, 2019. 1, 3
- [20] Sven Kosub. A note on the triangle inequality for the jaccard distance. *Pattern Recognition Letters*, 120:36–38, 2019. 5
- [21] James MacQueen et al. Some methods for classification and analysis of multivariate observations. In *Proceedings of the fifth Berkeley symposium on mathematical statistics and probability*, volume 1, pages 281–297. Oakland, CA, USA, 1967. 1
- [22] Robert Osada, Thomas Funkhouser, Bernard Chazelle, and David Dobkin. Shape distributions. *ACM Transactions on Graphics (TOG)*, 21(4):807–832, 2002. 3
- [23] Adam Paszke, Sam Gross, Francisco Massa, Adam Lerer, James Bradbury, Gregory Chanan, Trevor Killeen, Zeming

- Lin, Natalia Gimelshein, Luca Antiga, Alban Desmaison, Andreas Kopf, Edward Yang, Zachary DeVito, Martin Raison, Alykhan Tejani, Sasank Chilamkurthy, Benoit Steiner, Lu Fang, Junjie Bai, and Soumith Chintala. Pytorch: An imperative style, high-performance deep learning library. In H. Wallach, H. Larochelle, A. Beygelzimer, F. d'Alché-Buc, E. Fox, and R. Garnett, editors, *Advances in Neural Information Processing Systems 32*, pages 8024–8035. Curran Associates, Inc., 2019. 6
- [24] Charles R Qi, Hao Su, Kaichun Mo, and Leonidas J Guibas. Pointnet: Deep learning on point sets for 3d classification and segmentation. In *Proceedings of the IEEE conference on computer vision and pattern recognition*, pages 652–660, 2017. 1
- [25] Charles R Qi, Hao Su, Matthias Nießner, Angela Dai, Mengyuan Yan, and Leonidas J Guibas. Volumetric and multi-view cnns for object classification on 3d data. In *Proceedings of the IEEE conference on computer vision and pattern recognition*, pages 5648–5656, 2016. 1
- [26] Peter J Rousseeuw. Silhouettes: a graphical aid to the interpretation and validation of cluster analysis. *Journal of computational and applied mathematics*, 20:53–65, 1987. 5
- [27] Heung-Yeung Shum, Martial Hebert, and Katsushi Ikeuchi. On 3d shape similarity. In *Proceedings CVPR IEEE Computer Society Conference on Computer Vision and Pattern Recognition*, pages 526–531. IEEE, 1996. 3
- [28] Richard Socher, Brody Huval, Bharath Bath, Christopher D Manning, and Andrew Ng. Convolutional-recursive deep learning for 3d object classification. *Advances in neural information processing systems*, 25, 2012. 1
- [29] Hang Su, Subhransu Maji, Evangelos Kalogerakis, and Erik Learned-Miller. Multi-view convolutional neural networks for 3d shape recognition. In *Proceedings of the IEEE international conference on computer vision*, pages 945–953, 2015. 3, 4
- [30] Xuebin Sun, Han Ma, Yuxiang Sun, and Ming Liu. A novel point cloud compression algorithm based on clustering. *IEEE Robotics and Automation Letters*, 4(2):2132–2139, 2019. 1
- [31] Wouter Van Gansbeke, Simon Vandenhende, Stamatios Georgoulis, Marc Proesmans, and Luc Van Gool. Scan: Learning to classify images without labels. In *European Conference on Computer Vision*, pages 268–285. Springer, 2020. 5
- [32] Zhirong Wu, Shuran Song, Aditya Khosla, Fisher Yu, Linguang Zhang, Xiaoou Tang, and Jianxiong Xiao. 3d shapenets: A deep representation for volumetric shapes. In *Proceedings of the IEEE conference on computer vision and pattern recognition*, pages 1912–1920, 2015. 1
- [33] Junyuan Xie, Ross Girshick, and Ali Farhadi. Unsupervised deep embedding for clustering analysis. In *International conference on machine learning*, pages 478–487. PMLR, 2016. 5
- [34] Cong Yang and Marcin Grzegorzec. Object similarity by humans and machines. In *2014 AAAI Fall Symposium Series*, 2014. 3
- [35] Xiaohang Zhan, Jiahao Xie, Ziwei Liu, Yew-Soon Ong, and Chen Change Loy. Online deep clustering for unsupervised representation learning. In *Proceedings of the IEEE/CVF conference on computer vision and pattern recognition*, pages 6688–6697, 2020. 1
- [36] Cha Zhang and Yunqian Ma. *Ensemble machine learning: methods and applications*. Springer, 2012. 2, 6

A. Appendix

A.1. Challenges for class annotation

The challenges for annotating CAD models in the ABC dataset are mainly from three aspects: (1) a large proConsistency between annotatorsrtion of non-standard models, (2) complex and unbalanced class distributions, and (3) lack of units and texture information.

Large proConsistency between annotatorsrtion of non-standard models. We have four annotators to label 10,533 CAD models from the ABC dataset. Each annotator will give the model a label, indicating it is a standard or non-standard model. We then collect all the label information and use a majority voting strategy to determine the final label for each model. Note that if the number of the standard label and non-standard label for a model is the same, we discard the model annotation. Finally, we have 10,090 CAD models that can be considered to have a usable human label. The proConsistency between annotatorsrtion of the standard part and non-standard part can be seen in Table 6. We can see those non-standard models occupy around 45% of the data in our select dataset, showing that it is difficult to give class labels to almost half models in the dataset.

| Component Type | Count | Percentage |
|-------------------|-------|------------|
| Standard Part | 5671 | 56.20% |
| Non-Standard Part | 4419 | 43.80% |

Figure 6. **Large proportion of non-standard models.**

Complex and unbalanced class distributions. We also have four annotators to label the same 10,533 CAD models for class. We can find that the category distribution in the dataset is unbalanced 7. For example, industrial components occupy more than two-thirds of the models, while aerospace models and agriculture models only occupy 0.05%.

Lack of units and texture information. During the labeling process, our annotators report that for some CAD models, it is difficult to give them labels because of the lack of units or texture information.

A.2. Interfaces for 3D models annotation

We show the example for annotating cluster 251 in Figure 8. For the annotation round 1, the interface shows 12 CAD models with checkboxes (set to be checked). The annotator should manually unmark the models that are not similar to the checked models. Then after round 1, the checked models will be labeled as similar to each other, and the remaining models will be sent to the annotation round 2. We repetitively ask the annotator to unmark the checks, until the annotator believes that the remaining models are all dissimilar to each other such that no sub-cluster can be created.

| Product Category | Count | Percentage |
|------------------------|-------|------------|
| Aerospace | 5 | 0.05% |
| Agriculture | 5 | 0.05% |
| Automobile | 71 | 0.67% |
| Children Toy | 178 | 1.69% |
| Construction | 145 | 1.38% |
| Educational | 30 | 0.28% |
| Electronics | 200 | 1.90% |
| Electrical | 86 | 0.82% |
| Fishing | 13 | 0.12% |
| General Transportation | 66 | 0.63% |
| Home Goods | 411 | 3.90% |
| Industrial Component | 7111 | 67.51% |
| Medical Device | 66 | 0.63% |
| Oil & Gas | 10 | 0.09% |
| Paper Products | 37 | 0.35% |
| Wood & Furniture | 249 | 2.36% |
| None | 1850 | 17.56% |

Figure 7. **Unbalanced class distributions.**

A.3. Human annotator instruction and payment

As aforementioned, the human standard to determine the similarity relationship between every two CAD models relies on previous expert knowledge that is difficult to describe. We provided the following instructions to our human annotators, to help them be more consistent. First, the similarity should be determined by the geometry, instead of the functionality. Second, the annotators should assume that the similarity relationship is rotational and translational invariant. We pay the human annotators 10 dollars per hour. In total, we spent around 12,000 dollars for human annotations.

A.4. Human annotation data statistics

We show the Positive/negative/negative edge percentage of human annotation in Figure 9 and human label consistency in Figure 10 for both Option-A and Option-B. We find that: (1) different annotators might have different criteria to label the similarity relationships, since *Annotator#1* and *Annotator#3* give more negative labels than *Annotator#2* and *Annotator#4* (see Figure 9); (2) Even though the annotators' annotation criteria could be different, most of the labeling consistency between annotators shows that human can achieve consensus on the 3D model similarity judgment (see Figure 10). Therefore, we believe it is reasonable to use these human annotations.

A.5. Data processing

Point cloud generation. We process 3D CAD models to point cloud by sampling 4,096 points for each model, using Kaolin [17]. Then we apply min-max normalization to the sampled point cloud for each model.

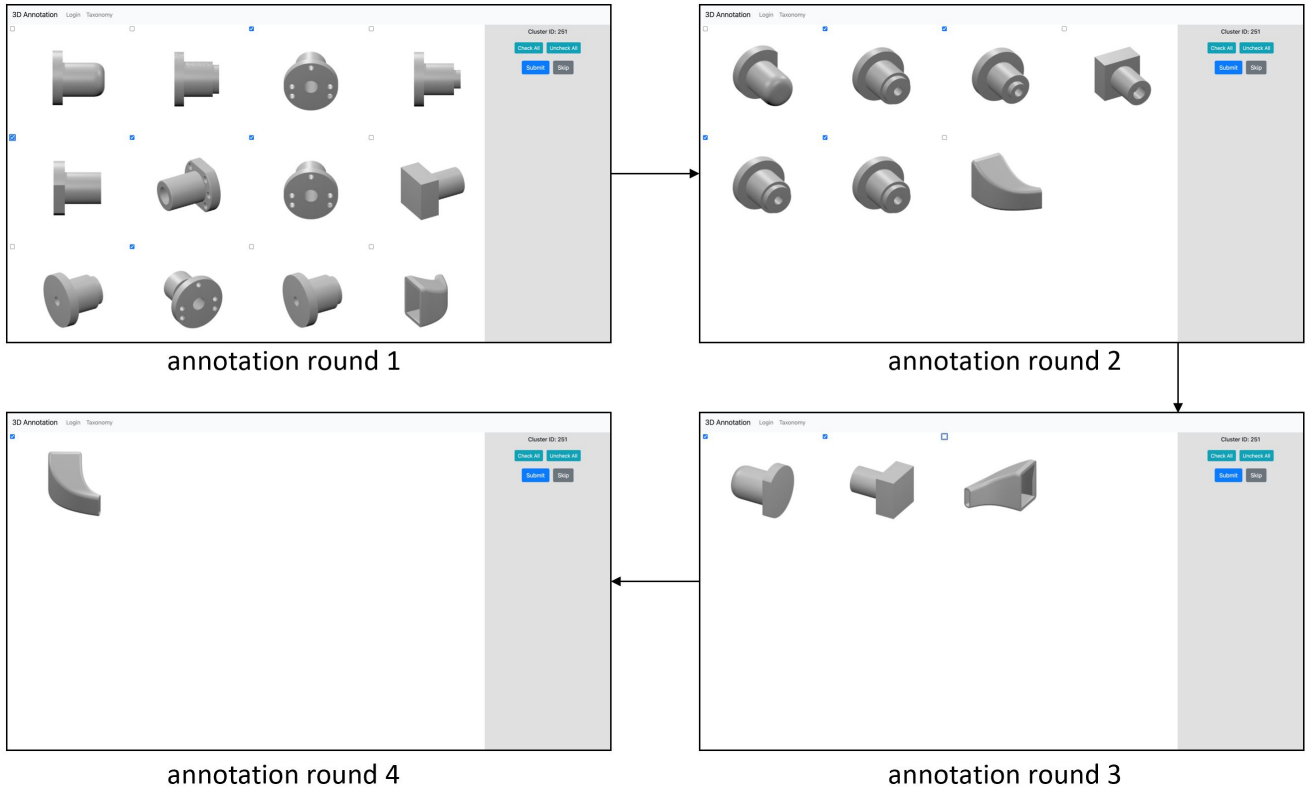


Figure 8. Annotation interface example.

| | | Annotator#1 | Annotator#2 | Annotator#3 | Annotator#4 |
|----------|----------------|-------------|-------------|-------------|-------------|
| Option-A | Positive Edges | 12.07% | 36.32% | 13.58% | 56.75% |
| | Negative Edges | 87.93% | 63.68% | 86.42% | 43.25% |
| Option-B | Positive Edges | 13.68% | 38.49% | 21.60% | 47.57% |
| | Negative Edges | 86.32% | 61.51% | 78.40% | 52.43% |

Figure 9. Positive/negative edge percentage.

Chamfer distance computation. The input of the Chamfer distance is the pre-processed point cloud for each CAD model that is normalized using min-max normalization (e.g. for each dimension, the min and max will be 0 and 1 after the normalization, and the scaling is affine).

Jaccard distance computation. Pairwise IoU (Intersection over Union, Jaccard index) of the objects are calculated first. The input of the IoU is voxel grids generated from the pre-processed point cloud for each CAD model that is normalized using min-max normalization. The IoU is not normalized for the case when the object is too thin to normalize, and thus the IoU of it versus anything will be zero. Then the Jaccard distance will be $1 - \text{IoU}$ by definition.

A.6. Network architectures

For all the baseline methods, we use the original code from their reConsistency baselines and just modify the backbone networks to adjust to our data. We will release our code online and more details of the network could be found there.

A.7. External evaluation indices

We detail the *edge accuracy* and *balanced accuracy* in this part.

Edge accuracy. It is natural to compare the edge clustering results with the annotated similarity matrix, which is the evaluation metric in correlation clustering [1]. We note

Option-A

| | Annotator#1 | Annotator#2 | Annotator#3 | Annotator#4 |
|-------------|-------------|-------------|-------------|-------------|
| Annotator#1 | - | 0.75120 | 0.95714 | 0.54874 |
| Annotator#2 | 0.75120 | - | 0.76648 | 0.74388 |
| Annotator#3 | 0.95714 | 0.76648 | - | 0.56400 |
| Annotator#4 | 0.54874 | 0.74388 | 0.56400 | - |

Average Consistency: 0.72190

Option-B

| | Annotator#1 | Annotator#2 | Annotator#3 | Annotator#4 |
|-------------|-------------|-------------|-------------|-------------|
| Annotator#1 | - | 0.74579 | 0.90619 | 0.65536 |
| Annotator#2 | 0.74579 | - | 0.80566 | 0.80543 |
| Annotator#3 | 0.90619 | 0.80566 | - | 0.72209 |
| Annotator#4 | 0.65536 | 0.80543 | 0.72209 | - |

Average Consistency: 0.77341

Figure 10. Consistency between annotators.

| | | Human Confusion Matrix | | | | | | | | | | | | | | | |
|-------------|------------------|------------------------|-----------------|-----------------|-----------------|-----------------|-----------------|-----------------|-----------------|-----------------|-----------------|-----------------|-----------------|-----------------|-----------------|--|--|
| | | K=32 | | K=64 | | K=128 | | K=256 | | K=512 | | K=1024 | | K=2000 | | | |
| | | Actual Positive | Actual Negative | Actual Positive | Actual Negative | Actual Positive | Actual Negative | Actual Positive | Actual Negative | Actual Positive | Actual Negative | Actual Positive | Actual Negative | Actual Positive | Actual Negative | | |
| AtlasNet | Predict Positive | 23.68% | 15.73% | 23.46% | 13.24% | 23.25% | 11.90% | 22.96% | 10.77% | 23.00% | 10.16% | 22.82% | 9.32% | 22.46% | 7.87% | | |
| | Predict Negative | 1.55% | 59.04% | 1.77% | 61.53% | 1.98% | 62.87% | 2.27% | 64.00% | 2.23% | 64.61% | 2.41% | 65.45% | 2.77% | 66.90% | | |
| BYOL | Predict Positive | 22.29% | 10.75% | 22.50% | 8.63% | 22.42% | 6.61% | 21.10% | 4.97% | 19.06% | 3.40% | 16.07% | 2.29% | 14.12% | 1.36% | | |
| | Predict Negative | 2.94% | 64.01% | 2.73% | 66.14% | 2.81% | 68.16% | 4.13% | 69.80% | 6.17% | 71.37% | 9.16% | 72.48% | 11.11% | 73.41% | | |
| DeepCluster | Predict Positive | 21.57% | 9.36% | 21.21% | 6.68% | 21.10% | 5.27% | 20.31% | 4.07% | 19.33% | 2.60% | 16.50% | 1.76% | 13.64% | 0.90% | | |
| | Predict Negative | 3.66% | 65.41% | 4.02% | 68.69% | 4.13% | 69.50% | 4.92% | 70.76% | 5.90% | 72.17% | 8.73% | 73.01% | 11.59% | 73.87% | | |
| DEC | Predict Positive | 23.26% | 14.67% | 23.14% | 12.27% | 23.14% | 11.10% | 22.93% | 9.33% | 22.71% | 8.21% | 22.19% | 7.19% | 21.81% | 5.39% | | |
| | Predict Negative | 1.97% | 60.10% | 2.09% | 62.50% | 2.09% | 63.67% | 2.30% | 65.44% | 2.52% | 66.56% | 3.04% | 67.58% | 3.42% | 69.38% | | |
| IIC | Predict Positive | 21.05% | 10.70% | 21.16% | 8.43% | 20.94% | 6.60% | 20.07% | 9.01% | 19.61% | 7.42% | 19.95% | 5.70% | 19.12% | 7.61% | | |
| | Predict Negative | 4.18% | 64.07% | 4.07% | 66.34% | 4.29% | 68.17% | 5.16% | 65.76% | 5.62% | 67.35% | 5.28% | 69.07% | 6.11% | 67.16% | | |
| SCAN | Predict Positive | 23.38% | 14.17% | 23.04% | 11.92% | 23.36% | 12.01% | 23.42% | 13.59% | 23.69% | 14.62% | 23.73% | 16.01% | 23.82% | 18.30% | | |
| | Predict Negative | 1.85% | 60.60% | 2.19% | 62.85% | 1.87% | 62.76% | 1.81% | 61.18% | 1.54% | 60.15% | 1.50% | 58.76% | 1.41% | 56.47% | | |
| MVCNN | Predict Positive | 8.48% | 2.88% | 8.15% | 1.53% | 7.98% | 0.84% | 7.88% | 0.43% | 7.83% | 0.23% | 7.81% | 0.14% | 7.80% | 0.08% | | |
| | Predict Negative | 16.75% | 71.89% | 17.08% | 73.24% | 17.25% | 73.93% | 17.35% | 74.34% | 17.40% | 74.54% | 17.42% | 74.63% | 17.43% | 74.69% | | |

| | | Ensemble Confusion Matrix | | | | | | | | | | | | | | | |
|-------------|------------------|---------------------------|-----------------|-----------------|-----------------|-----------------|-----------------|-----------------|-----------------|-----------------|-----------------|-----------------|-----------------|-----------------|-----------------|--|--|
| | | K=32 | | K=64 | | K=128 | | K=256 | | K=512 | | K=1024 | | K=2000 | | | |
| | | Actual Positive | Actual Negative | Actual Positive | Actual Negative | Actual Positive | Actual Negative | Actual Positive | Actual Negative | Actual Positive | Actual Negative | Actual Positive | Actual Negative | Actual Positive | Actual Negative | | |
| AtlasNet | Predict Positive | 0.94% | 3.69% | 0.49% | 1.67% | 0.33% | 0.82% | 0.19% | 0.36% | 0.12% | 0.22% | 0.08% | 0.13% | 0.05% | 0.09% | | |
| | Predict Negative | 0.08% | 95.29% | 0.06% | 97.78% | 0.03% | 98.83% | 0.02% | 99.42% | 0.01% | 99.65% | 0.01% | 99.78% | 0.00% | 99.86% | | |
| BYOL | Predict Positive | 0.71% | 2.62% | 0.40% | 1.42% | 0.26% | 0.66% | 0.13% | 0.33% | 0.07% | 0.18% | 0.04% | 0.11% | 0.03% | 0.07% | | |
| | Predict Negative | 0.31% | 96.36% | 0.15% | 98.03% | 0.10% | 98.99% | 0.08% | 99.46% | 0.06% | 99.69% | 0.04% | 99.81% | 0.03% | 99.88% | | |
| DeepCluster | Predict Positive | 0.52% | 2.96% | 0.27% | 1.52% | 0.18% | 0.70% | 0.10% | 0.33% | 0.06% | 0.17% | 0.03% | 0.09% | 0.02% | 0.04% | | |
| | Predict Negative | 0.50% | 96.02% | 0.28% | 97.93% | 0.18% | 98.94% | 0.11% | 99.46% | 0.07% | 99.70% | 0.05% | 99.83% | 0.04% | 99.90% | | |
| DEC | Predict Positive | 0.85% | 3.76% | 0.47% | 1.73% | 0.30% | 0.78% | 0.19% | 0.36% | 0.11% | 0.18% | 0.08% | 0.09% | 0.05% | 0.07% | | |
| | Predict Negative | 0.17% | 95.22% | 0.08% | 97.73% | 0.06% | 98.86% | 0.03% | 99.43% | 0.02% | 99.69% | 0.01% | 99.82% | 0.00% | 99.88% | | |
| IIC | Predict Positive | 0.65% | 5.37% | 0.38% | 4.45% | 0.24% | 3.58% | 0.15% | 5.04% | 0.10% | 6.07% | 0.07% | 3.56% | 0.05% | 6.02% | | |
| | Predict Negative | 0.37% | 95.61% | 0.17% | 95.00% | 0.12% | 96.06% | 0.06% | 94.74% | 0.03% | 93.80% | 0.02% | 96.35% | 0.01% | 93.92% | | |
| SCAN | Predict Positive | 0.87% | 2.67% | 0.49% | 1.50% | 0.34% | 1.35% | 0.21% | 3.39% | 0.13% | 5.46% | 0.08% | 6.82% | 0.06% | 9.49% | | |
| | Predict Negative | 0.14% | 96.31% | 0.06% | 97.96% | 0.02% | 98.29% | 0.01% | 96.40% | 0.00% | 94.41% | 0.00% | 95.10% | 0.00% | 90.46% | | |
| MVCNN | Predict Positive | 0.09% | 3.76% | 0.03% | 2.03% | 0.01% | 1.14% | 0.01% | 0.59% | 0.01% | 0.33% | 0.00% | 0.19% | 0.00% | 0.11% | | |
| | Predict Negative | 0.93% | 95.22% | 0.52% | 97.42% | 0.35% | 98.50% | 0.20% | 99.19% | 0.12% | 99.54% | 0.08% | 99.72% | 0.05% | 99.83% | | |

Figure 11. Confusion matrices on Human and Ensemble.

that the similarity matrix is an undirected graph $\mathcal{G}(\mathcal{V}, \mathcal{E})$ on N nodes. Let e_{ij} denote the label of the edge relationship between object i, j , and $e_{ij} = e_{ji}$. $E = \{e_{ij}\}$ denote all the edges. $G' = (V', E')$ is the subgraph of G , which is only comConsistency based of the known labels. $E' = \{e_{ij} | e_{ij} = 1 \vee e_{ij} = -1, e_{ij} \in E\}$. For the clustering results obtained from the baseline methods, \hat{e}_{ij}

denote the clustered edge relationship between object i, j . If objects i, j are grouped into the same cluster, we assume the two objects are similar, therefore $\hat{e}_{ij} = 1$. Otherwise $\hat{e}_{ij} = -1$. The edge accuracy is defined as: $\text{acc} = \sum_{e_{ij} \in E'} \frac{|\hat{e}_{ij} - e_{ij}|}{2n(E')}$, where $n(E')$ is the number of elements in E' . The range of the edge accuracy is $[0, 1]$.

Balanced accuracy. Unlike *edge accuracy* that might

suffer from the unbalanced dataset, balanced accuracy can be used to better evaluate the methods' performance. Specifically, for each baseline method, after having all the edge relationships \hat{e}_{ij} in E' , we generate a confusion matrix that can be used to calculate balanced accuracy. The detailed information for balanced accuracy can be found in [2].

A.8. Human and Ensemble confusion matrices

Table 11 shows all the confusion matrices generated using both *Human* and *Ensemble* matrices. Note that we use percentage representations in the confusion matrices for a more intuitive understanding of the performance of one baseline method.